

Supporting Online Material for

Fermionic Superfluidity with Imbalanced Spin Populations

Martin W. Zwierlein,* André Schirotzek, Christian H. Schunck,
Wolfgang Ketterle

*To whom correspondence should be addressed. E-mail: zwierlei@mit.edu

Published 22 December 2005 on *Science Express*
DOI: 10.1126/science.1122318

This PDF file includes:

Materials and Methods
Figs. S1 and S2
References and Notes

Fermionic Superfluidity with Imbalanced Spin Populations

Martin W. Zwierlein, André Schirotzek, Christian H. Schunck,
Wolfgang Ketterle

Materials and Methods

Creation of ultracold imbalanced spin mixtures. To map out the superfluid regime as a function of population imbalance, we use two complementary techniques: the detection of vortices in a rotating cloud (*S1*) and the determination of the fraction of condensed fermion pairs in non-rotating mixtures (*S2–S4*). The two experimental methods require slightly different procedures for imaging the pair condensate wavefunction after release from the trap. To determine the fraction of condensed vs uncondensed pairs, the condensate must separate well from the thermal cloud and should therefore remain small. For the detection of rotating clouds, the condensate should expand to a large size in order to magnify the vortices. In the following, we give the parameters used to determine the condensate fraction (experiment B) in parentheses after those used for vortex detection (experiment A).

In the first stage of the experiment, fermionic ${}^6\text{Li}$ atoms were sympathetically cooled to degeneracy by ${}^{23}\text{Na}$ atoms in a magnetic trap (*S5*). The ultracold cloud was subsequently loaded into an optical dipole trap (waist $w \approx 120 \mu\text{m}$) at a maximum trap depth of about $8 \mu\text{K}$. At a magnetic bias field of 875 G, a variable spin-mixture of the two lowest hyperfine states (labelled $|1\rangle$ and $|2\rangle$) was created via a Landau-Zener radiofrequency sweep with an adjustable sweep rate. The spin mixture was evaporatively cooled further by lowering the trap depth to $1.6 \mu\text{K}$ resulting in radial and axial trap frequencies of $\nu_r = 110 \text{ Hz}$ and $\nu_a = 23 \text{ Hz}$, respectively. At the same time, the magnetic field was ramped to about 815 G, which is on the BEC-side close to the Feshbach resonance at 834 G (*S6*), and deep in the strongly interacting regime. The rather moderate evaporation still leaves room for thermal molecules in an equal mixture, but was chosen to efficiently cool highly asymmetric mixtures, avoiding spilling of large Fermi clouds. This ensured that the total number of atoms was approximately constant and independent of the asymmetry between the two spin states (see Fig. S1).

For the vortex experiment, we set the spin mixture in rotation using two blue-detuned laser beams (wavelength 532 nm) rotated symmetrically around the cloud at angular frequency $\Omega = 2\pi 70 \text{ Hz}$ (*S1*). After 800 ms of stirring, the rotating cloud was left to equilibrate for several hundred ms (*S7*).

Tuning the interactions and imaging the cloud. Starting with either the rotating or the non-rotating cloud, we varied the interaction strength between the two spin states in the gas by ramping the magnetic field in 100 ms (experiment B: 500 ms) to several values around the Feshbach resonance (for the condensate fraction experiment B, the trap depth was simultaneously increased to $4 \mu\text{K}$ ($\nu_r = 192 \text{ Hz}$)). After 50 ms (B: 100 ms) of hold time, an image of the cloud was taken following the procedure outlined in (S1): After releasing the cloud from the optical trap the binding energy of fermion pairs was rapidly increased by ramping the magnetic field within 2 ms (B: 200 μs) to 690 G, in the far wings of the resonance on the BEC side. Here, fermion pairs were stable throughout further expansion. After a total of 11 ms (B: 14 ms) of expansion (in the remaining magnetic saddle-point potential) an image of either state $|1\rangle$ or state $|2\rangle$ was taken. In experiment A on vortices, the clouds were imaged at 690 G. For the condensate fraction data (B), the magnetic field was suddenly switched to 800 G right before imaging. At this field the molecules absorb the probe light with the same strength as free atoms (reduced to 75% at 690 G). The images revealed the center-of-mass wavefunction of the pairs and, for rotating clouds, eventually the presence of vortices. For the condensate fraction experiment, the 200 μs fast ramp to the BEC-side immediately after release from the trap ensured that even large condensates separated well from the normal, uncondensed component. A rapid ramp to zero field would result in an even better separation (S3, S4), but we found that field sweeps into regions far outside the resonance cause loss of observed atoms (S4). Since the ramp was fast compared to the radial trapping period, the size of the expanded condensate was mostly governed by the residual mean-field interaction at 690 G, where $a = 1400 a_0$. This expanded size was actually smaller than that of a condensate released from equilibrium at 690 G, because of the lower mean-field energy before expansion.

The described approach to detect fermion pair condensates originating from the BCS-side was theoretically discussed by several authors (S8–S12). In some cases (S8, S10, S11) even quantitative agreement with experiments (S2, S3) was reached. It is reasonable to assume that condensed fermion pairs on the BCS-side can transform into zero-momentum molecules, as long as their original pair size is smaller than the interparticle spacing. Experimentally, our group showed that the formation dynamics of these condensates is slow compared to the time needed to cross resonance in the rapid ramp (S4), excluding growth of the condensate during the ramp. The ramp employed in our present work does not result in loss of atoms, previously encountered for ramps to zero field (S4). The condensate fraction is thus a direct measure of the superfluid component in the mixture.

Determining the condensate fraction. Fig. S2 shows typical optical density profiles originating from resonance. Azimuthal averaging resulted in very good signal-to-noise in the optical density, with relative fluctuations of 10^{-3} . The total signal fluctuated from shot-to-shot by about 5%, due to frequency fluctuations of the imaging laser, but the profile's shape was not affected. Imperfections in the polarization of the light, stray light etc. tend to systematically lower the optical density. Indeed, the total signal obtained by imaging with circularly polarized light along the magnetic field axis was 20% smaller than the (more robust) number obtained from imaging perpendicular to the magnetic field axis. The latter coincided with the total number of atoms, which was calibrated by measuring the trap frequencies and the Fermi radius of almost perfectly spin-polarized degenerate Fermi clouds (a pure spin-polarized Fermi gas would not reach thermal equilibrium due to Pauli suppression of collisions).

The profile of the minority component was very well fit by a bimodal fit, consisting of a gaussian $e^{-r^2/2R_{\text{th}}^2}$ plus a Thomas-Fermi-profile of the form $(1 - x^2)^{3/2}$ for the condensate. The standard deviation in the condensate fraction for three measurements taken over the course of an hour was 1%, while the standard deviation of the population imbalance was 3%. A more refined fitting function, accounting for depletion of the thermal cloud in the presence of the condensate, increased the condensate fraction by at most 10% (for a condensate fraction of 50%), without changing the quality of the fit (see Fig. S2).

The highest condensate fractions of 40% were limited by the chosen evaporation ramp, which avoided spilling of large Fermi clouds but did not result in the coldest attainable temperatures for equal mixtures (see Fig. S1). Essentially pure condensates, with no appreciable thermal component, were achieved in equal mixtures by evaporating to a lower final trap depth. For asymmetric mixtures, such a ramp strongly reduces the population imbalance by preferentially removing unpaired atoms.

Thermometry in the strongly interacting regime. The width of the expanded thermal molecular cloud R_{th} after the rapid ramp to the BEC-side provides an upper limit for the system's temperature (see Fig. S1). The average radial kinetic energy per molecule in the thermal cloud is given by $E_{\text{kin}} = 2mR_{\text{th}}^2/t^2$, where m is the mass of a lithium atom and t is the expansion time. A standard correction was applied to this formula accounting for the cloud's expansion in the harmonic saddle-point potential. For a non-interacting cloud, E_{kin}/k_B equals the temperature of the gas, where k_B is Boltzmann's constant. Interactions increase E_{kin} . Note, however, that the mixture immediately after the rapid ramp to the BEC-side is more dilute than an equilibrium sample at 690 G, due to the large initial size of the Fermi gas on the BCS-side. E_{kin}/k_B should therefore be a good estimate of the system's temperature. Indeed, for equal mixtures on resonance, a condensate was observed when E_{kin}/E_F (E_F is the Fermi energy of an equal mixture) was lowered from 0.34 (diamonds in Fig. 4, 833 G) to 0.28 (triangles in Fig. 4). This is close to the predictions $T_C/T_F = 0.29$ (S13), $T_C/T_F = 0.31$ (S14) and $T_C/T_F = 0.3$ (S15) for the ratio of the critical temperature of superfluidity on resonance and the Fermi temperature $T_F = E_F/k_B$.

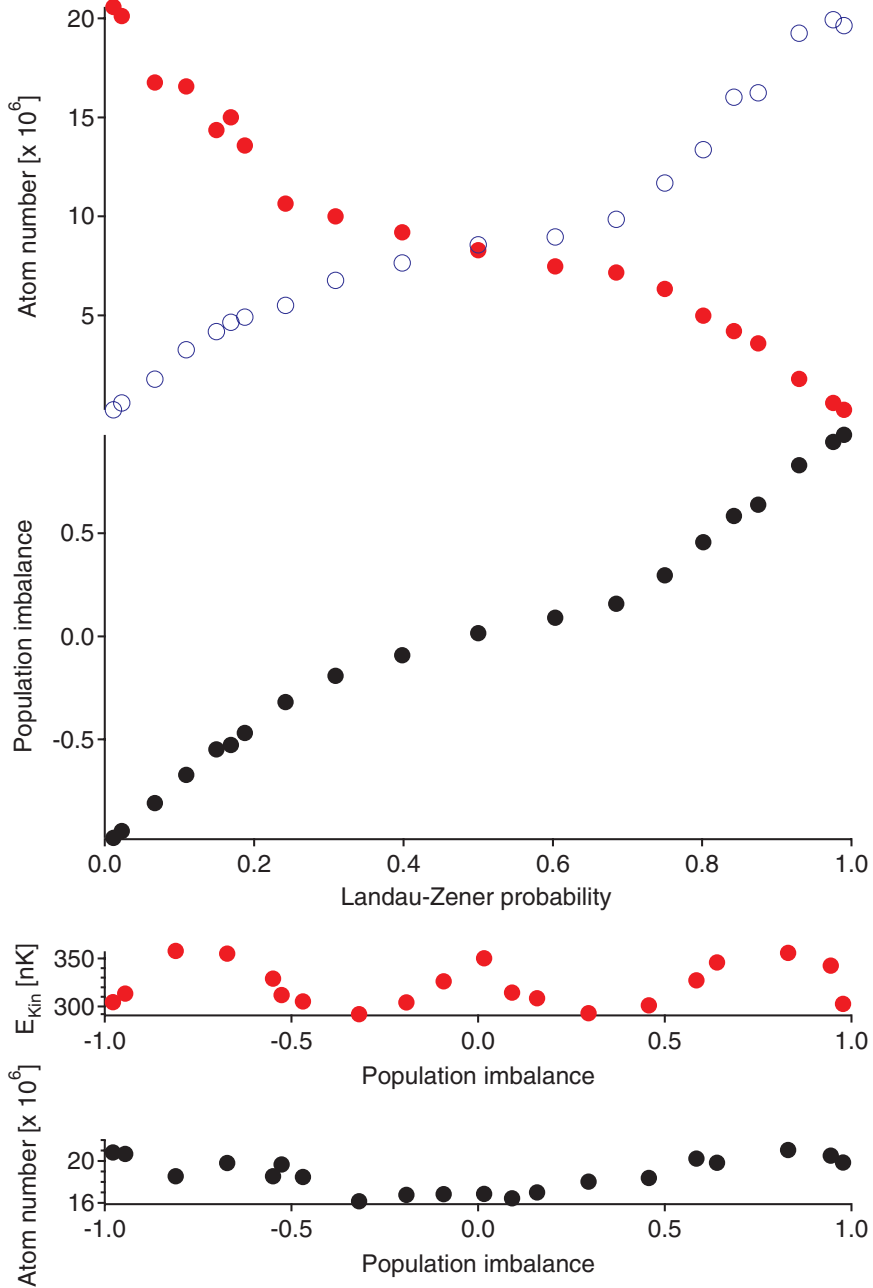


Figure 1: Upper two panels: Dependence of the spin populations after evaporation and their imbalance as a function of the rate of the radiofrequency sweep applied to control the spin populations at full trap depth. These sweeps are characterized by their Landau-Zener transfer probability. Lower panels: Dependence of the average radial kinetic energy and the total number of atoms in the mixture as a function of population imbalance. The clouds originate from 883 G (BCS-side, see Fig. 4). Red closed circles: Atoms in state $|1\rangle$. Open blue circles: Atoms in state $|2\rangle$. The data-points are averages of three measurements taken over the course of one hour.

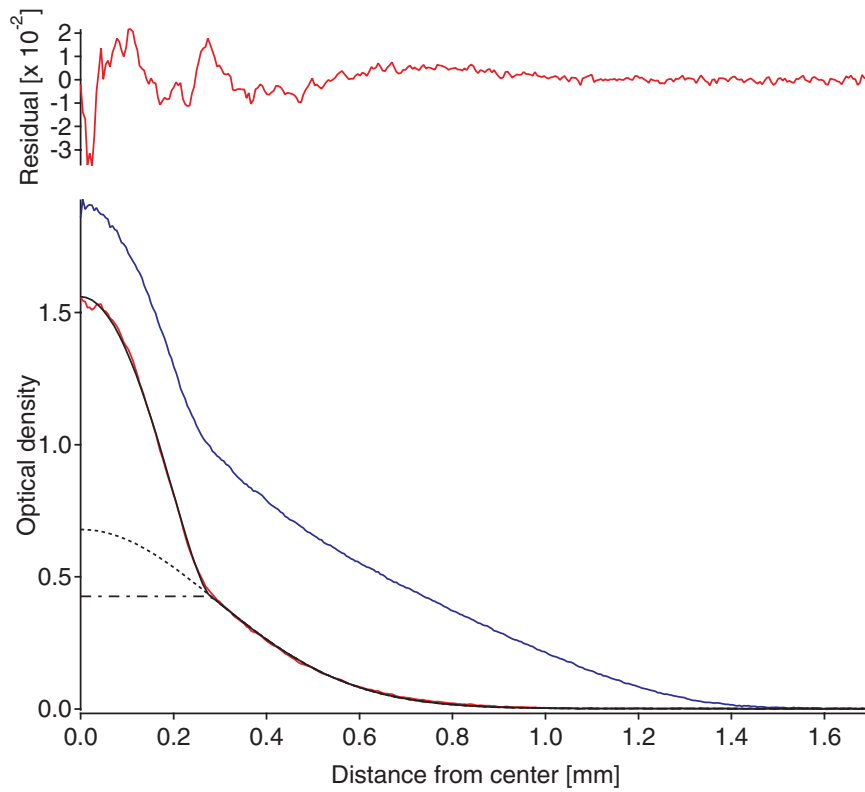


Figure 2: Radial density profiles of an unequal spin mixture originating from resonance. The density profile of the minority component (red curve) was fit using two different models for the thermal cloud: the non-interacting case (gaussian, dotted line) and the strongly interacting case of a thermal cloud that is fully separated from the condensate (leading to a flat distribution in the axially integrated profile at points where there is a condensate, dash-dotted line). The two fits are indistinguishable on the scale of this graph. The residual of the gaussian plus Thomas-Fermi-fit after subtraction of the original profile is shown on top.

References and Notes

- S1. M. W. Zwierlein, J. R. Abo-Shaeer, A. Schirotzek, C. H. Schunck, W. Ketterle, *Nature* **435**, 1047 (2005).
- S2. C. A. Regal, M. Greiner, D. S. Jin, *Phys. Rev. Lett.* **92**, 040403 (2004).
- S3. M. W. Zwierlein, *et al.*, *Phys. Rev. Lett.* **92**, 120403 (2004).
- S4. M. W. Zwierlein, C. H. Schunck, C. A. Stan, S. M. F. Raupach, W. Ketterle, *Phys. Rev. Lett.* **94**, 180401 (2005).
- S5. Z. Hadzibabic, *et al.*, *Phys. Rev. Lett.* **91**, 160401 (2003).
- S6. M. Bartenstein, *et al.*, *Phys. Rev. Lett.* **94**, 103201 (2004).
- S7. Note that due to damping in our not perfectly round trap, the mixture will rotate at a speed lower than Ω . The vortex number in an equal mixture around 875 G (BCS-side) decayed with a time constant of 3 s. Asymmetric spin mixtures should spin down faster, due to the increased friction exerted by the non-superfluid component.
- S8. T.-L. Ho. Preprint cond-mat/0404517.
- S9. A. V. Avdeenkov, J. L. Bohn, *Phys. Rev. A* **71**, 023609 (2005).
- S10. A. Perali, P. Pieri, G. C. Strinati, *Phys. Rev. Lett.* **95**, 010407 (2005).
- S11. L. Salasnich, N. Manini, A. Parola, *Phys. Rev. A* **72**, 023621 (2005).
- S12. E. Altman, A. Vishwanath, *Phys. Rev. Lett.* **95**, 110404 (2005).
- S13. J. Kinast, *et al.*, *Science* **307**, 1296 (2005).
- S14. A. Perali, P. Pieri, L. Pisani, G. C. Strinati, *Phys. Rev. Lett.* **92**, 220404 (2004).
- S15. G. M. Bruun, H. Smith, *Phys. Rev. A* **72**, 043605 (2005).